

The inositol 5-phosphatase SHIP2 is an effector of RhoA and is involved in cell polarity and migration

Katsuhiko Kato^{a,b}, Tsubasa Yazawa^a, Kentaro Taki^a, Kazutaka Mori^{a,b}, Shujie Wang^{a,c}, Tomoki Nishioka^a, Tomonari Hamaguchi^a, Toshiki Itoh^d, Tadaomi Takenawa^e, Chikako Kataoka^f, Yoshiharu Matsuura^f, Mutsuki Amano^a, Toyooki Murohara^b, and Kozo Kaibuchi^a

^aDepartment of Cell Pharmacology and ^bDepartment of Cardiology, Nagoya University Graduate School of Medicine, 65 Tsurumai, Showa, Nagoya, Aichi 466-8550, Japan; ^cDepartment of Anatomy, School of Medicine, Mie University, 2-174 Edobashi, Tsu, Mie 514-8507, Japan; ^dDivision of Membrane Biology and ^eDivision of Lipid Biochemistry, Department of Biochemistry and Molecular Biology, Kobe University Graduate School of Medicine, 7-5-1 Kusunoki, Chuo, Kobe, Hyogo 650-0017, Japan; ^fDepartment of Molecular Virology, Research Institute for Microbial Diseases, Osaka University, 3-1, Yamadaoka, Suita, Osaka 565-0871, Japan

ABSTRACT Cell migration is essential for various physiological and pathological processes. Polarization in motile cells requires the coordination of several key signaling molecules, including RhoA small GTPases and phosphoinositides. Although RhoA participates in a front–rear polarization in migrating cells, little is known about the functional interaction between RhoA and lipid turnover. We find here that src-homology 2–containing inositol-5-phosphatase 2 (SHIP2) interacts with RhoA in a GTP-dependent manner. The association between SHIP2 and RhoA is observed in spreading and migrating U251 glioma cells. The depletion of SHIP2 attenuates cell polarization and migration, which is rescued by wild-type SHIP2 but not by a mutant defective in RhoA binding. In addition, the depletion of SHIP2 impairs the proper localization of phosphatidylinositol 3,4,5-trisphosphate, which is not restored by a mutant defective in RhoA binding. These results suggest that RhoA associates with SHIP2 to regulate cell polarization and migration.

Monitoring Editor
Tamotsu Yoshimori
Osaka University

Received: Nov 29, 2011
Revised: Apr 10, 2012
Accepted: May 8, 2012

INTRODUCTION

Cell migration plays an important role in tissue development, immune function, and wound healing. Most migrating cells have a highly polarized morphology, such as a front leading edge and rear tail, and front–rear polarity is critical for the efficiency of cell migration (Ridley *et al.*, 2003; Petrie *et al.*, 2009). One of the major regulators of front–rear polarity is the Rho family of small GTPases, including

Rho, Rac, and Cdc42. The activities of Rho GTPases are controlled in a temporal and spatial manner to regulate actin cytoskeleton reorganization, cell polarity, and migration (Jaffe and Hall, 2005). RhoA is mainly activated in the rear and central regions to promote the assembly and activation of contractile actomyosin networks and to restrict protrusions. RhoA is also activated at the leading edge (Kurokawa and Matsuda, 2005; Pertz *et al.*, 2006). Rac1 and Cdc42 are predominantly activated at the leading edge to generate a vectorial protrusion in the direction of migration (Kraynov *et al.*, 2000; Itoh *et al.*, 2002). These Rho GTPases regulate various cellular functions through downstream effectors. Rho-kinase/ROCK/ROK, which is one of the best-characterized effectors of RhoA, is believed to be a key regulator of front–rear polarity (Riento and Ridley, 2003; Narumiya *et al.*, 2009; Amano *et al.*, 2010). Rho-kinase phosphorylates Par-3, a component of the Par polarity complex, or FilGAP, the negative regulator for Rac, resulting in Rac1 inactivation (Ohta *et al.*, 2006; Nakayama *et al.*, 2008). In addition to Rho-kinase, other RhoA effectors might also be involved in front–rear polarity, because the cell

This article was published online ahead of print in MBoC in Press (<http://www.molbiolcell.org/cgi/doi/10.1091/mbc.E11-11-0958>) on May 16, 2012.

Address correspondence to: Kozo Kaibuchi (kaibuchi@med.nagoya-u.ac.jp).

Abbreviations used: FN, fibronectin; LC-MS/MS, liquid chromatography–tandem mass spectrometry; PI3K, phosphatidylinositol 3-kinase; PI(3,4,5)P₃, phosphatidylinositol 3,4,5-trisphosphate; PLA, proximity ligation assay.

© 2012 Kato *et al.* This article is distributed by The American Society for Cell Biology under license from the author(s). Two months after publication it is available to the public under an Attribution–Noncommercial–Share Alike 3.0 Unported Creative Commons License (<http://creativecommons.org/licenses/by-nc-sa/3.0>).

“ASCB®,” “The American Society for Cell Biology®,” and “Molecular Biology of the Cell®” are registered trademarks of The American Society of Cell Biology.

morphology phenotype of cells treated with the Rho-kinase inhibitor was different from that of RhoA-depleted cells (Figure 1B).

Another key regulator of front–rear polarity is the cellular phosphoinositide signaling system. Among the phosphoinositides, phosphatidylinositol 3,4,5-trisphosphate (PI(3,4,5)P₃) accumulates at the front of directionally migrating cells (Ridley *et al.*, 2003). PI(3,4,5)P₃ is produced by the phosphorylation of PI(4,5)P₂ by a family of enzymes known as phosphatidylinositol 3-kinases (PI3Ks) and regulates the localization of specific proteins by binding to their pleckstrin homology domains (Cantley, 2002). The levels of phospholipids are tightly regulated by kinases, phosphatases, and phospholipases (Di Paolo and De Camilli, 2006). Interactions between Rho GTPases and phosphoinositide metabolism are implicated in cell polarity. However, the details of how Rho GTPases and phosphoinositide signaling are coordinated remain unclear.

In this study, we performed affinity chromatography to search for effectors of RhoA involved in front–rear polarity. We identified several candidates of novel RhoA effectors, including src-homology 2–containing inositol-5-phosphatase 2 (SHIP2), a PI(3,4,5)P₃-5 phosphatase. SHIP2 directly interacted with GTP-bound but not GDP-bound RhoA. SHIP2 appeared to restrict PI(3,4,5)P₃ localization at the leading edge in migrating cells to thereby control the cell polarity downstream of RhoA. We demonstrate a novel linkage between Rho family GTPases and lipid signaling via a SHIP2–RhoA interaction in the establishment of cell polarity.

RESULTS

Front–rear polarity and the Rho pathway

When suspended cells, such as Vero fibroblasts and U251 glioma cells, are plated on extracellular matrix proteins, the cells begin to spread. Next the cells begin to ruffle, with the accumulation of actin filaments around the cell periphery, the so-called lamellipodia, and develop membrane extensions. Then the lamellipodia gradually divide into several regions. Finally, the lamellipodia localize to one side, and the cells acquire a distinct front–rear polarized morphology. Polarized cells have a single leading edge with an accumulation of actin filaments. In this study, we used U251 glioma cells because they have a distinct front–rear polarized morphology and persistently migrate when seeded on a fibronectin (FN)-coated surface (Figure 1A).

To investigate the roles of the Rho pathway in front–rear polarity, we first compared RhoA knockdown with Y-27632 treatment, a specific Rho-kinase inhibitor. RhoA-depleted cells or cells treated with Y-27632 were suspended and seeded on FN-coated glasses. Approximately 40% of U251 cells transfected with control siRNA had a single leading edge with a polarized morphology 8 h after plating (Figure 1B). Cells with a single leading edge were observed less in both RhoA-depleted cells and cells treated with Y-27632. RhoA-depleted cells had an elongated cell shape or an extended, flattened morphology with multiple small protrusions, whereas cells treated with Y-27632 had long, thin processes and flattened, elongated protrusions without stress fibers (Figure 1B). Given that the cell morphology phenotype of cells treated with Y-27632 did not resemble that of RhoA knockdown, RhoA regulates cell polarity through not only Rho-kinase, but also other effectors.

SHIP2 as a novel effector of RhoA

To explore the other RhoA effectors involved in front–rear polarity, we attempted to identify novel RhoA effectors with RhoA affinity column chromatography followed by a liquid chromatography–tandem mass spectrometry (LC-MS/MS) shotgun analysis. We prepared GDP-RhoA, GTPγS (a nonhydrolyzable GTP analogue)-RhoA, and RhoA mutants (RhoA-L63, constitutively active mutant; RhoA-N19,

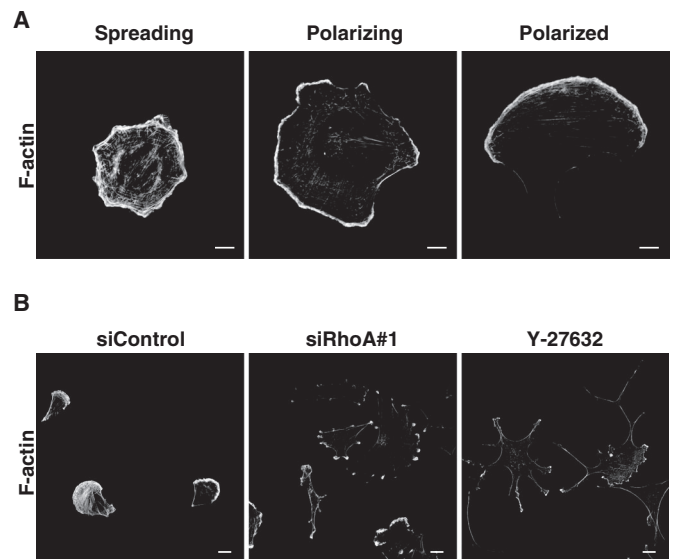


FIGURE 1: Regulation of front–rear polarity downstream of RhoA. (A) Polarization of U251 cells. U251 cells were plated on FN-coated glass and stained with Alexa 488–phalloidin. Bar, 10 μm. (B) Effect of RhoA depletion or Y-27632 treatment in U251 cells. U251 cells transfected with the indicated siRNAs for 72 h were treated with or without 20 μM Y-27632, reseeded on FN-coated glasses for 8 h, fixed, and stained with Alexa 488–phalloidin. Bar, 20 μm. All results are representative of at least three independent experiments.

dominant-negative mutant) as glutathione S-transferase (GST)–fusion proteins and used them as ligands for the affinity columns. A cytosolic fraction of rat heart was applied to affinity beads coated with GST alone or GST-RhoA mutants. Numerous proteins were detected in the eluates from the columns coated with GST-RhoA mutants (Figure 2A). Eluates from the GST and GST-RhoA mutant affinity columns were used for shotgun analysis using LC-MS/MS. The list of representative RhoA-interacting proteins is shown in Supplemental Table S1. Several known effectors, including Rho-kinase, PKN, Rhotekin, and MYPT1, were detected in the eluates from the GTPγS-GST-RhoA and active GST-RhoA-L63 columns (Supplemental Table S1).

In addition to the known RhoA-interacting proteins, we identified many proteins that specifically interacted with the GTPγS-bound active form or active mutant of RhoA but not the GDP-bound inactive form or dominant-negative mutant. Some of these proteins appear to be novel effectors of RhoA. Several proteins, including acetyl-coenzyme A acetyltransferase 1 (ACAT1), SHIP2, filamin A interacting protein (FILIP), and striatin, calmodulin-binding protein 3 (STRN3), were identified as candidate effectors. To confirm the amounts of these proteins in eluates, we performed immunoblot analysis using specific antibodies (Figure 2B). The bands recognized by the anti-Rho-kinase antibody were detected in the eluates from the GTPγS-GST-RhoA- and GST-RhoA-L63-immobilized columns but not in those from the GST-, GDP-GST-RhoA-, or GST-RhoA-N19-immobilized columns. RhoGDI was detected in the eluates of the GDP-GST-RhoA-immobilized column. Consistent with the mass spectrometric analysis, ACAT1 and SHIP2 were detected in the eluates from the GTPγS-GST-RhoA- and GST-RhoA-L63-immobilized columns (Figure 2B). SHIP2 dephosphorylates PI(3,4,5)P₃ into phosphatidylinositol 3,4-bisphosphate. SHIP2 is believed to be a negative regulator of PI3K pathways; in addition, it regulates the actin cytoskeleton and is involved in cell migration, cell adhesion, endocytosis, and metastasis of cancer (Ooms *et al.*, 2009). We decided to

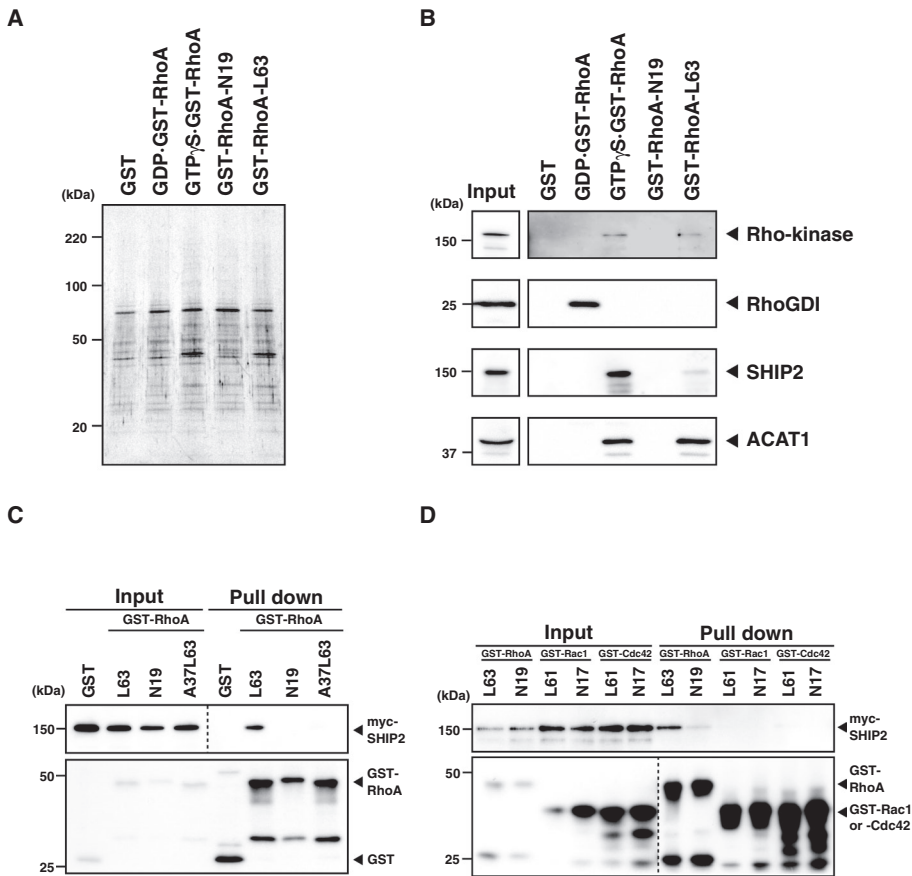


FIGURE 2: Identification of RhoA-binding proteins. (A) Isolation of RhoA-binding proteins by affinity column chromatography. GST, GDP-GST-RhoA, GTP γ S-GST-RhoA, or GST-RhoA mutants were immobilized on beads and incubated with the rat heart lysate. The bound proteins were eluted with buffer containing 1 M NaCl and subjected to SDS-PAGE, followed by silver staining. (B) Validation of LC-MS/MS results by immunoblotting. The eluates from affinity column chromatography were subjected to immunoblotting using anti-Rho-kinase, anti-RhoGDI, anti-SHIP2, and anti-ACAT1 antibodies. (C) Interaction of SHIP2 with active RhoA in COS7 cells. Glutathione-Sepharose beads were incubated with COS7 cell lysate expressing both myc-SHIP2 and GST-RhoA mutants. The bound proteins were analyzed by immunoblotting with anti-myc and anti-GST antibodies. The dashed line indicates separate membranes. (D) Specific interaction of SHIP2 with RhoA but not Rac1 or Cdc42. Glutathione-Sepharose beads were incubated with COS7 cell lysate expressing both myc-SHIP2 and GST-RhoA, GST-Rac1, or GST-Cdc42 mutants. The bound proteins were analyzed by immunoblotting with anti-myc and anti-GST antibodies. All results are representative of at least three independent experiments.

focus on SHIP2 because it is involved in cell polarity and actin polymerization.

Characterization of SHIP2-RhoA binding

To determine whether SHIP2 associates with active RhoA in COS7 cells, we performed pull-down assays using the constitutively active RhoA mutant. Extracts of COS7 cells cotransfected with myc-SHIP2 and GST or GST-RhoA mutants were prepared and mixed with glutathione-Sepharose beads. SHIP2 interacted with GST-RhoA-L63 but not GST, GST-RhoA-N19, or GST-RhoA-A37L63, which contains an amino acid substitution in the effector domain and has no ability to bind the effectors (Figure 2C). These results suggest that SHIP2 is a novel effector of RhoA.

Among the 10 mammalian inositol polyphosphate 5-phosphatases, SHIP1 and SHIP2 are structurally similar proteins with high sequence identity (Ooms *et al.*, 2009). To examine whether SHIP1 also associates with active RhoA, we performed binding assays and

found that SHIP1 did not interact with active RhoA under the same experimental conditions (Supplemental Figure S1A). We also found that SHIP2 was expressed in U251 glioma, MDA-MB-231 epithelial, and RAW264.7 macrophage cells, whereas SHIP1 was expressed in RAW264.7 macrophage cells but was undetectable in U251 and MDA-MB-231 cells (Supplemental Figure S1B), suggesting that SHIP2 is a major SHIP in U251 and MDA-MB-231 cells. To reveal the signal linkage between SHIP2 and Rho family GTPases, we assessed the specificity of their interactions and confirmed that SHIP2 specifically interacted with RhoA but not Rac1 or Cdc42 (Figure 2D).

Direct interaction of SHIP2 with active RhoA

To narrow down the RhoA-binding region in SHIP2, we generated several SHIP2 fragments (Figure 3A) and found that green fluorescent protein (GFP)-SHIP2-N interacted with GTP γ S-GST-RhoA, whereas GFP-SHIP2-cat or C did not (Figure 3B). To further narrow down and confirm the direct interaction of active RhoA with SHIP2, we performed an *in vitro* binding assay. GST-, GDP-GST-RhoA-, and GTP γ S-GST-RhoA-immobilized beads were incubated with each maltose-binding protein (MBP)-SHIP2 fragment. GTP γ S-GST-RhoA interacted with MBP-SHIP2-N and MBP-SHIP2-N Δ SH2 but not MBP-SHIP2-SH2 (Figure 3C). The SHIP2-N Δ SH2-4 fragment (124–314 amino acids) was sufficient to bind to RhoA (Supplemental Figure S2A). These results indicate that active RhoA directly interacts with SHIP2 at the N-terminal region between the SH2 and catalytic domains. The binding activity of SHIP2-N Δ SH2-4 fragment was comparable with that of the Rho-kinase-Rho-binding (RB) fragment containing RhoA-binding domain (Supplemental Figure S2B).

We next examined whether the SHIP2-N Δ SH2-4 contains a conserved binding motif to RhoA. It has been shown that PKN/PRK1 interacts with RhoA through a leucine zipper-like motif (Maesaki *et al.*, 1999). Because SHIP2-N Δ SH2-4 contains this motif, it could be important for RhoA binding (Supplemental Figure S2C). A series of SHIP2 point mutants (D193/E195A, S202/N203A, R216/R217A, and D223/K224A) was generated based on several reports regarding structure and mutation analysis (Peck *et al.*, 2002; Owen *et al.*, 2003; Shimizu *et al.*, 2003; Blumenstein and Ahmadian, 2004). The binding activities of MBP-SHIP2-N Δ SH2-4-D193/E195A and D223/K224A to active RhoA were much lower than that of MBP-SHIP2-N Δ SH2-4 under these conditions (Supplemental Figure S2D). We then generated a full-length SHIP2-D193/E195A mutant; the binding activity of myc-SHIP2-D193/E195A for active RhoA was dramatically reduced compared with myc-SHIP2-wild type (WT) (Figure 3D). These results suggest that the leucine zipper-like motif in the N-terminus of SHIP2 is necessary for RhoA binding.

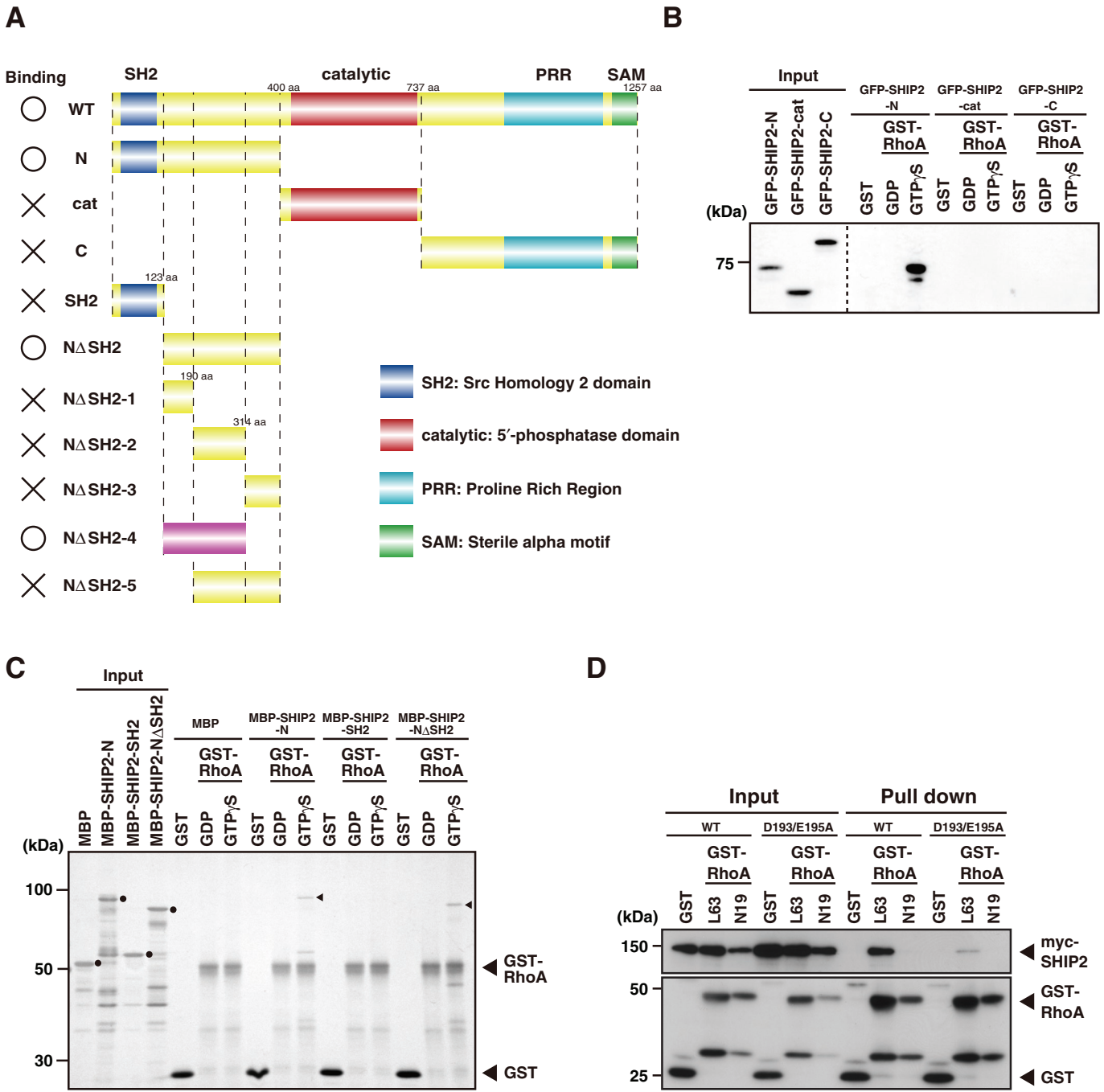


FIGURE 3: Interaction of SHIP2 with active RhoA. (A) Domain structure and deletion constructs of SHIP2. (B) Mapping of the SHIP2 region required for binding to active RhoA. GST, GDP-GST-RhoA, or GTP γ S-GST-RhoA, immobilized on beads, was incubated with COS7 cell lysate expressing GFP-SHIP2-N, GFP-SHIP2-cat, or GFP-SHIP2-C. The bound proteins were analyzed by immunoblotting with the anti-GFP antibody. (C) Direct binding of SHIP2 with active RhoA. GST, GDP-GST-RhoA, or GTP γ S-GST-RhoA, immobilized on beads, was incubated with various MBP-SHIP2 fragments. The bound proteins were analyzed by silver staining. Black dots indicate respective intact bands, and arrowheads indicate the bound proteins. (D) Characterization of binding-deficient mutants of SHIP2 in COS7 cells. Glutathione-Sepharose beads were incubated with COS7 cell lysate expressing both myc-SHIP2-WT or myc-SHIP2-D193/E195A and GST-RhoA mutants. The bound proteins were analyzed by immunoblotting with anti-myc and anti-GST antibodies. All results are representative of at least three independent experiments.

To determine whether active RhoA could modulate the PI(3,4,5)P₃ 5-phosphatase activity of SHIP2, we performed *in vitro* phosphatase assays and found that GTP γ S-GST-RhoA did not affect the PI(3,4,5)P₃ 5-phosphatase activity of SHIP2 under the specific experimental conditions (Supplemental Figure S3).

We further addressed the function of SHIP2-RhoA interaction. When both myc-SHIP2 and control vector were transfected in U251 cells, most of the myc-SHIP2 was detected in the cytosol fraction. Coexpression with HA-RhoA-L63 increased the amount of myc-SHIP2 in the membrane fractions, whereas coexpression with

HA-RhoA-N19 or HA-RhoA-L63S190, which is an active RhoA mutant with mutation at the prenylation site and thereby fails to target the membrane, had minimal effect (Supplemental Figure S4A). We next asked whether RhoA could recruit SHIP2 in U251 cells using a strategy to engage RhoA on the mitochondria. Expression of a GFP (EGFP)-RhoA-L63 fused with mitochondrial targeting sequence (MitoEGFP-RhoA-L63) in U251 cells partly recruited SHIP2-mCherry to the mitochondria, whereas that of MitoEGFP-RhoA-N19 or MitoEGFP in U251 cells did not (Supplemental Figure S4B). These results suggest that RhoA can tether SHIP2 to the juxtamembrane region in an activity-dependent manner, where SHIP2 catalyzes the hydrolysis of PI(3,4,5)P₃.

Association of SHIP2 with RhoA in intact cells

To examine the subcellular localization of SHIP2 and RhoA, we immunostained U251 cells seeded on FN-coated glasses with anti-SHIP2 and anti-RhoA antibodies. SHIP2 and RhoA were partially colocalized at both the central region and leading edge in U251 cells (Figure 4A). To test the specificity of the anti-SHIP2 and anti-RhoA antibodies, endogenous SHIP2 and RhoA were depleted by two independent small interfering RNAs (siRNAs) or siRNA mixtures. The staining of SHIP2 and RhoA was strongly reduced upon knockdown of the proteins by siRNA (Supplemental Figure S5, A and B). We also confirmed that depletion of SHIP2 did not affect the RhoA activity in U251 cells (Supplemental Figure S5C). To examine whether SHIP2 associates with RhoA in intact U251 cells, we performed proximity ligation assays (PLAs). PLA allows for the detection of native complexes with minimal cellular disruption (Fredriksson *et al.*, 2002; Soderberg *et al.*, 2006). A signal is obtained only if oligonucleotides coupled to two separate antibodies are sufficiently close to allow enzymatic ligation; detection then relies on amplification from the ligated template, followed by hybridization with a fluorescent probe. This assay reveals protein interactions in intact cells. We detected many ubiquitous signals in the presence of the SHIP2 and RhoA antibodies, whereas few signals were obtained in the presence of the SHIP2 or RhoA antibody alone (Figure 4B). These signals were assumed to be the SHIP2–RhoA interaction. Furthermore, the spots of the SHIP2–RhoA interaction were reduced in RhoA-depleted cells (Figure 4B). We also observed many signals using Rho-kinase and RhoA antibodies (Supplemental Figure S5D). Quantitative analysis revealed that the signals of the SHIP2–RhoA interaction were more pronounced than the background obtained with each SHIP2 or RhoA antibody alone and the signals in RhoA-depleted cells (Figure 4C). These results indicate that SHIP2 associates with RhoA in intact U251 cells.

To further explore the interaction between SHIP2 and RhoA, we performed PLAs during cell spreading and polarization. When U251 cells were plated on FN-coated glasses, lamellipodia extension was promoted after 30 min to 1 h. Cells initiated polarization ~1 h after spreading. After polarization, cells finally acquired a distinct front–rear polarized morphology and began to migrate. Many signals were ubiquitously detected with PLAs, and SHIP2 and RhoA were partially colocalized at both the central region and the cell periphery during cell spreading and polarization, as detected by immunostaining (Figure 4D). These results suggest that an association between SHIP2 and RhoA is present during spreading and polarization.

We then tried to observe the localization of PI(3,4,5)P₃ because PI(3,4,5)P₃ is a key signaling molecule that becomes rapidly and highly polarized in cells, such as spreading cells (Weiger *et al.*, 2009). We observed PI(3,4,5)P₃ accumulation throughout the cell periphery 30 min and 1 h after plating. After initiation of polarization, the distribution of PI(3,4,5)P₃ tended to localize at actin accumulation

sites (Figure 4D). In addition, the distribution of PI(3,4,5)P₃ seemed different from that of the SHIP2–RhoA interaction.

Regulation of cell polarity by SHIP2 and RhoA

To examine the roles of SHIP2 and RhoA in cell polarization, we performed SHIP2 and RhoA siRNA knockdown in U251 cells. Cells depleted of SHIP2 or RhoA were suspended and seeded on FN-coated glasses. U251 cells depleted of SHIP2 were less polarized than controls and had spreading cell shapes (Figure 5A and Supplemental Figure S6A). These phenotypes were not resistant to treatment with Y-27632, which led to similar phenotypes. Phalloidin staining revealed that F-actin was observed at the peripheral regions of SHIP2-depleted cells, whereas RhoA-depleted cells became thinner and had multiple small, irregular protrusions (Figures 1B and 5A). Multiple small protrusions were also observed in RhoA-depleted PC3 prostate cancer cells during spreading (Vega *et al.*, 2011).

To examine the functional significance of the interaction of SHIP2 with RhoA, we performed rescue experiments. The expression of siRNA-resistant (RNAi^r)-SHIP2-WT rescued the polarization defects, whereas RNAi^r-SHIP2-D193/E195A or D608A, a phosphatase-deficient mutant, did not fully rescue the defects (Figure 5, B and C, and Supplemental Figure S6, B and C), suggesting that the RhoA-binding and phosphatase activities of SHIP2 are required for cell polarization. Similar observations were obtained in MDA-MB-231 epithelial cells (Supplemental Figure S7, A and B). We did not observe the phenotype of the overexpression of SHIP2-WT, possibly due to toxicity. Moderate expression of SHIP2-WT did not affect cell polarization. In addition, the overexpression of RhoA-WT and RhoA-L63 induced cell rounding.

Next we attempted to examine the effect of SHIP2 or RhoA knockdown on the localization of PI(3,4,5)P₃, because the depletion of SHIP1 or SHIP2 affects the levels or localization of PI(3,4,5)P₃ in several cell types (Blero *et al.*, 2005; Mandl *et al.*, 2007; Nishio *et al.*, 2007; Nakatsu *et al.*, 2010). The local accumulation of PI(3,4,5)P₃ at the leading edge is crucial to maintain front–rear polarity (Ridley *et al.*, 2003). Accumulation of PI(3,4,5)P₃ was observed at the leading edge in control U251 cells, whereas PI(3,4,5)P₃ was observed throughout the cell periphery in SHIP2-knockdown cells. In RhoA-knockdown cells, PI(3,4,5)P₃ did not accumulate at the leading edge and was instead found as multiple small, irregular protrusions (Figure 6, A and B, and Supplemental Figure S6D). PI(3,4,5)P₃ staining was markedly diminished in LY294002-treated cells (Figure 6A and Supplemental Figure S6D) or in cells overexpressing GFP-tagged SHIP2 or PTEN (Supplemental Figure S8). Furthermore, the expression of RNAi^r-SHIP2-WT rescued the restricted accumulation, whereas RNAi^r-SHIP2-D193/E195A or D608A did not fully rescue the accumulation (Figure 6, C and D, and Supplemental Figure S6, E and F). Similar observations were obtained in MDA-MB-231 epithelial cells (Supplemental Figure S7, C and D). These results suggest that SHIP2 regulates the proper localization of PI(3,4,5)P₃ downstream of RhoA, leading to the maintenance of cell polarity.

Requirement of the RhoA-binding activity of SHIP2 for cell migration

Finally, to examine the functional significance of the interaction between SHIP2 and RhoA in cell migration, we used a Boyden chamber assay. U251 cells transfected with either the indicated siRNA or siRNA along with indicated RNAi^r-SHIP2 were subjected to the Boyden chamber assay for 2 h. The depletion of SHIP2 or RhoA significantly impaired epidermal growth factor (EGF)-stimulated cell migration from the upper to the lower membrane. The two different

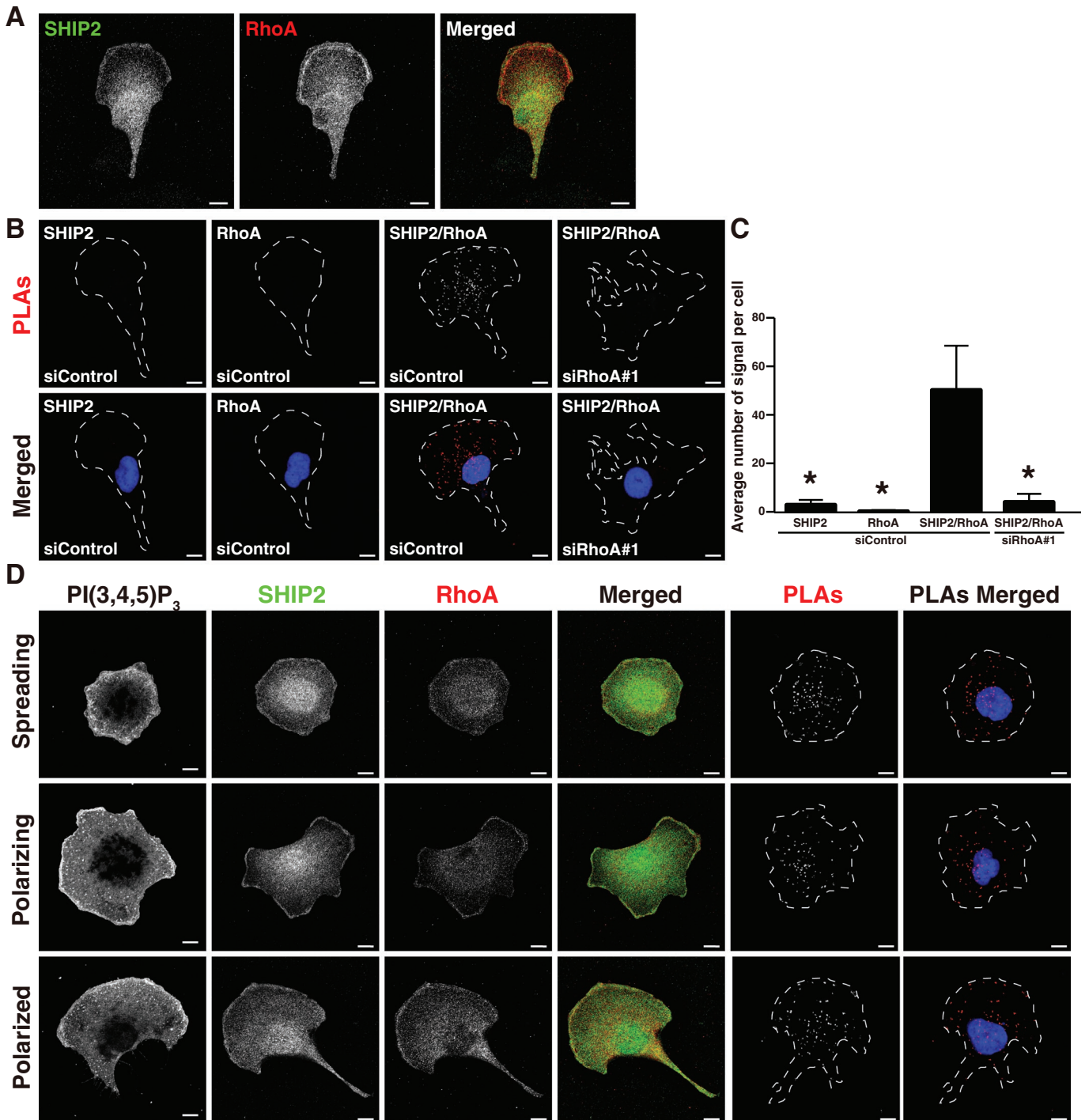


FIGURE 4: Association of SHIP2 with RhoA in intact cells. (A) Localization of SHIP2 and RhoA in U251 cells. U251 cells were double labeled with anti-SHIP2 (green) and anti-RhoA (red) antibodies. Right, the merged image. Bar, 10 μ m. (B) Association of SHIP2 with RhoA by proximity ligation assays in U251 cells. U251 cells were treated with control siRNA or siRNA against RhoA. PLA was performed using antibodies against SHIP2, RhoA, or both. Images represent focused views of several confocal sections that covered the entire region of cells. Cell edges are marked with a dotted line. Nuclei were stained with 4',6'-diamidino-2-phenylindole (DAPI; blue). Bar, 10 μ m. (C) Quantification of PLAs. Quantification of PLAs conducted in B. Asterisks indicate a difference from the value of SHIP2/RhoA PLA cells at $p < 0.01$. Error bars indicate \pm SD. (D) Association of SHIP2 with RhoA by PLA in spreading U251 cells. U251 cells were suspended and seeded on FN-coated glasses and fixed at 30 min and 1, 2, 4, and 8 h after plating. PLA was performed using antibodies against both SHIP2 and RhoA. Cells were stained with anti-PI(3,4,5)P₃, anti-RhoA, and anti-SHIP2 antibodies. PLA images represent focused views of several confocal sections that covered the entire region of cells. Cell edges are marked by a dotted line. Nuclei were stained with DAPI (blue). Bar, 10 μ m. All results are representative of at least three independent experiments. At least 50 cells were counted per experiment.

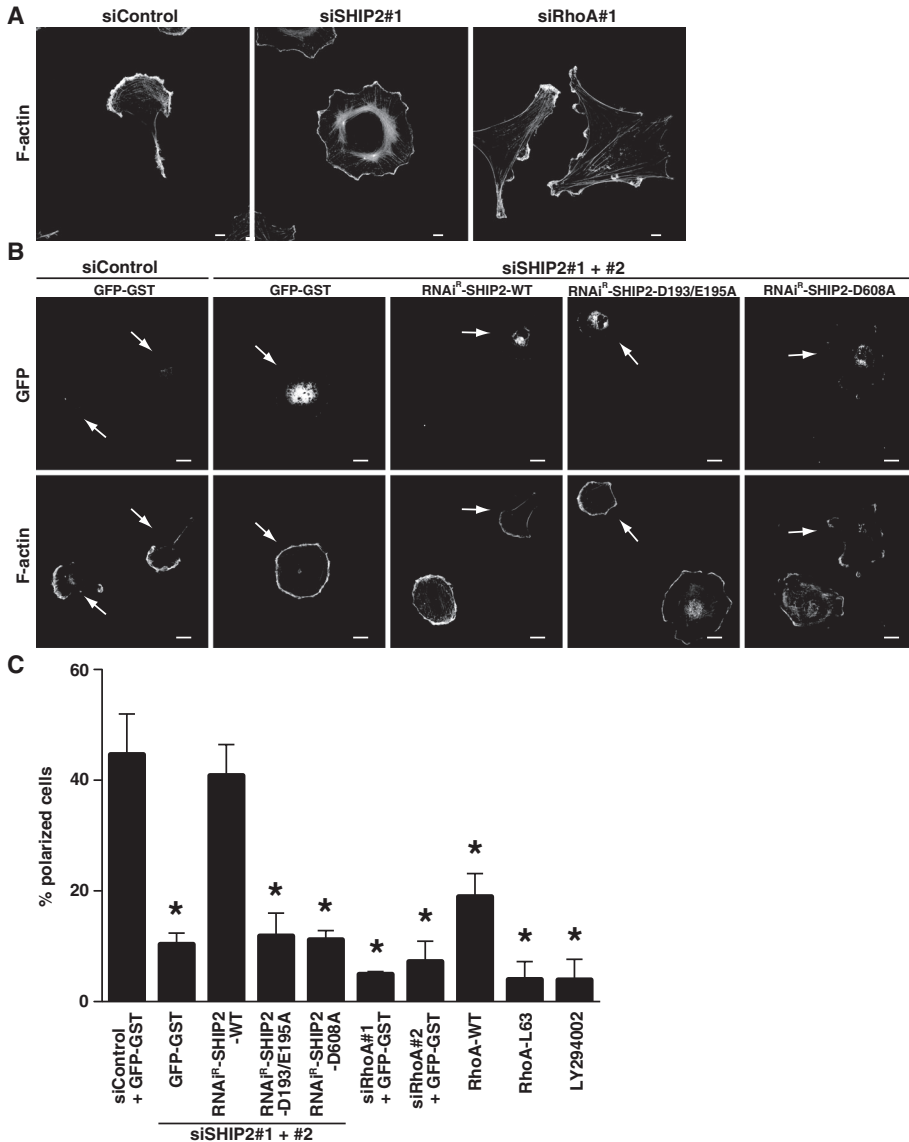


FIGURE 5: Requirement of SHIP2 for proper polarization in U251 cells. (A) Effect of the depletion of SHIP2 and RhoA in U251 cells. U251 cells transfected with the indicated siRNAs for 72 h were reseeded on FN-coated glasses for 8 h, fixed, and stained with tetramethylrhodamine isothiocyanate (TRITC)-phalloidin. Bar, 10 μ m. (B) Rescue experiments of SHIP2 knockdown in U251 cells. U251 cells transfected with both the indicated siRNAs and plasmids were reseeded on FN-coated glasses for 8 h, fixed, and stained with TRITC-phalloidin and the anti-GFP antibody. White arrows indicate transfected cells. Bar, 20 μ m. (C) Quantification of the effects of SHIP2 and RhoA mutants on cell polarity. The percentage of the cells that had a single leading edge is shown. Asterisks indicate a difference from the value of control cells at $p < 0.01$. Error bars indicate \pm SD. All results are representative of at least three independent experiments. At least 100 cells were counted per experiment.

sets of siRNAs to SHIP2 and RhoA showed similar effects on cell migration. The inhibitory effect of SHIP2 depletion was rescued by the expression of RNAi^R-SHIP2-WT but not by the expression of RNAi^R-SHIP2-D193/E195A or D608A (Figure 7), suggesting that the interaction of RhoA and SHIP2 is required for cell migration.

DISCUSSION

In this study, we identified several novel RhoA effector candidates, including SHIP2, by affinity chromatography of the GTP-bound form of RhoA. The N-terminal domain of SHIP2 directly and specifically interacted with the GTP-bound, but not GDP-bound, RhoA. The

proximity ligation assays revealed the association of SHIP2 with RhoA in U251 cells. The depletion of SHIP2 impaired not only the front-rear polarity and polarized distribution of PI(3,4,5)P₃ but also cell migration. Wild-type SHIP2 rescued the SHIP2-knockdown phenotypes, including defects in front-rear polarity and haptotactic migration, whereas the SHIP2 mutant defective in RhoA binding could not rescue these phenotypes. Thus SHIP2 appears to regulate PI(3,4,5)P₃ levels and restrict its localization to a single site, thereby controlling cell polarity and cell migration downstream of RhoA.

Rho family GTPases, including RhoA, Rac1, and Cdc42, have been implicated in establishing the front-rear polarity of migrating cells. Rac1 and Cdc42 are predominantly activated at the front leading edge to generate a vectorial protrusion. The leading protrusion is stabilized by its adherence to the surrounding extracellular matrix through adhesion receptors, such as integrins, which in turn induces PI(3,4,5)P₃ production and thereby activates Rac1 and Cdc42 through guanine nucleotide exchange factors (GEFs) to further induce new protrusions (Rameh *et al.*, 1997; Han *et al.*, 1998). PI(3,4,5)P₃ controls the localization of DOCK2, a GEF for Rac, leading to the regulation of membrane translocation and Rac activation (Kunisaki *et al.*, 2006). PI(3,4,5)P₃ also activates Akt to maintain the actin stress fibers and cortical actin filaments for directional cell migration through Girdin, a downstream substrate of Akt (Weng *et al.*, 2010). In contrast, RhoA activity is mainly activated in the central and rear regions, which may ensure front-rear polarity (Jaffe and Hall, 2005; Etienne-Manneville, 2008; Iden and Collard, 2008). RhoA is believed to inhibit Rac1 activity, thereby preventing ectopic protrusion in the rear region (Worthylake and Burridge, 2003). It has been reported that RhoA inhibits the Rac1 activity acting via Rho-kinase to phosphorylate FilGAP and Par-3 (Ohta *et al.*, 2006; Nakayama *et al.*, 2008). Rho-kinase also phosphorylates myosin phosphatase and inactivates it, thereby increasing the phosphorylation of myosin light chain and

activating myosin II (Kimura *et al.*, 1996), which may inhibit Rac1 activity through Rac1 GEF (Lee *et al.*, 2010). In addition to Rho-kinase, we found that RhoA maintains the proper localization and levels of PI(3,4,5)P₃ via SHIP2 in migrating cells, thereby contributing to the establishment of front-rear polarity.

How does RhoA regulate SHIP2 functions? We examined the effect of RhoA on the phosphatase activity of SHIP2 in a cell-free system and found that the GTP-bound RhoA did not affect phosphatase activity toward PI(3,4,5)P₃ under our assay conditions, suggesting that RhoA does not modulate the enzymatic activity of SHIP2 (Supplemental Figure S3). However, we cannot rule out the possibility

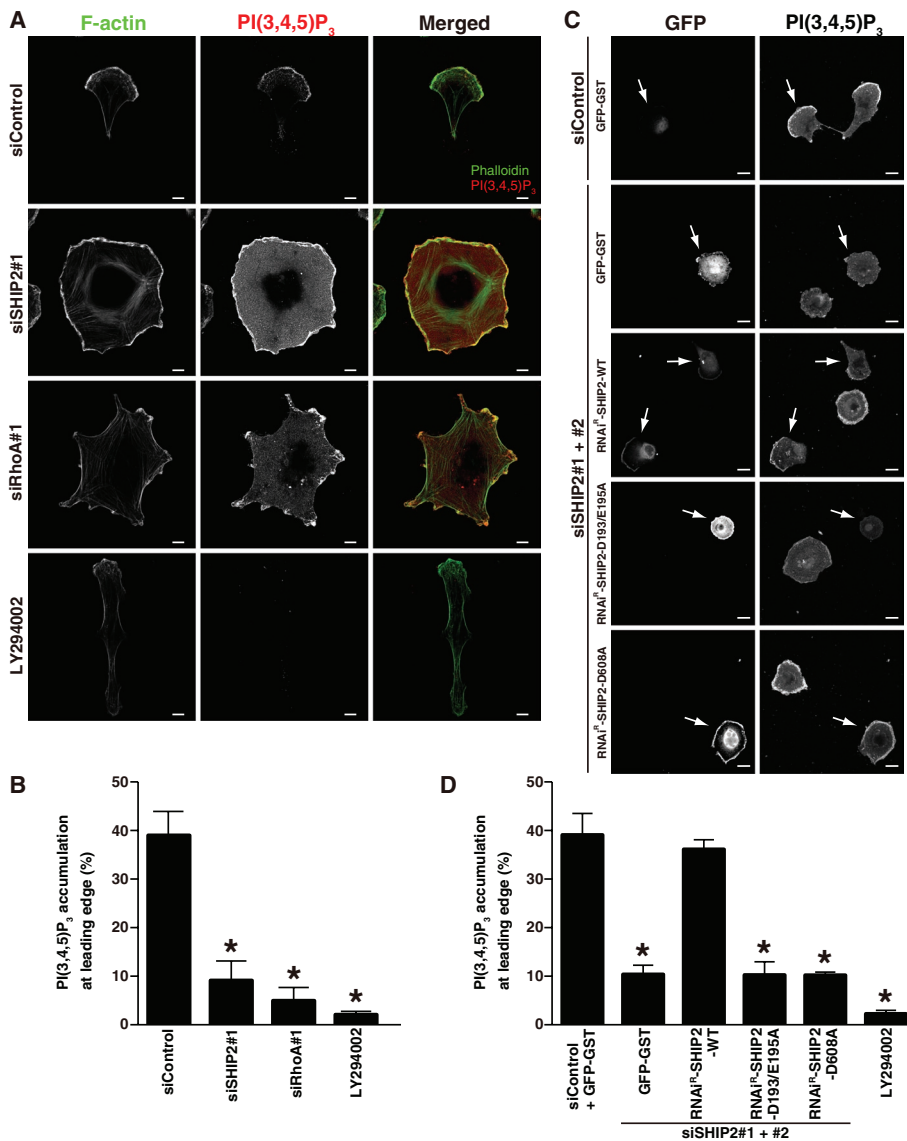


FIGURE 6: Requirement of SHIP2 for the proper accumulation of PI(3,4,5)P₃. (A) PI(3,4,5)P₃ localization in SHIP2- or RhoA-depleted U251 cells. U251 cells transfected with the indicated siRNAs for 72 h were reseeded on FN-coated glasses for 8 h, cultured for 1 h in the presence or absence of 50 μM LY294002, fixed, and stained with Alexa 488–phalloidin and the anti-PI(3,4,5)P₃ antibody. Bar, 10 μm. (B) Quantification of the effects of SHIP2 or RhoA knockdown on the accumulation of PI(3,4,5)P₃ at the leading edge. The percentage of the cells in which the accumulation of PI(3,4,5)P₃ was observed at a single leading edge is shown. Asterisks indicate a difference from the value of control cells at $p < 0.01$. Error bars indicate \pm SD. (C) Rescue experiments of SHIP2 knockdown in U251 cells. U251 cells transfected with both the indicated siRNAs and plasmids were reseeded on FN-coated glasses for 8 h, fixed, and stained with anti-PI(3,4,5)P₃ and anti-GFP antibodies. White arrows indicate transfected cells. Bar, 20 μm. (D) Quantification of the effects of SHIP2 knockdown and rescue mutants on the accumulation of PI(3,4,5)P₃ at the leading edge. The percentage of the cells in which the accumulation of PI(3,4,5)P₃ was observed at a single leading edge is shown. Asterisks indicate a difference from the value of control cells at $p < 0.01$. Error bars indicate \pm SD. All results are representative of at least three independent experiments. At least 100 cells were counted per experiment.

that we cannot satisfactorily reconstitute the *in vivo* situation with purified RhoA and SHIP2. Because RhoA-binding activity is required for SHIP2 to control cell polarization and migration (Figures 5, B and C, and 7) and SHIP2 is partly recruited by RhoA in a RhoA activity-dependent manner (Supplemental Figure S4), RhoA may be needed to properly localize SHIP2 at the membranes to prevent the overproduction of PI(3,4,5)P₃, which may inhibit ectopic protrusion. We

speculate that RhoA functions as a cutoff filter for PI(3,4,5)P₃ to suppress ectopic accumulation through local regulation of SHIP2 activity and/or localization. The SHIP2–RhoA interaction was observed ubiquitously in cells (Figure 4B), but we could not identify the exact cellular compartments in which the PLA signals were located due to the low resolution of this analysis. The distribution of PI(3,4,5)P₃ was found not only at the plasma membrane, but also localized to endocytosed vesicles, nuclei, and intracellular membranes (Sato *et al.*, 2003; Horiguchi *et al.*, 2006; Lindsay *et al.*, 2006). Of note, we cannot exclude the possibility that polarized PI(3,4,5)P₃ localization is disturbed as the consequence of disruption in polarized leading edge formation or other molecules in the regulation and localization of SHIP2 are involved. Further analysis of the site of colocalization is necessary to understand the link between SHIP2 and RhoA signaling.

In addition to SHIP2, we identified novel RhoA effector candidates, including ACAT1, FILIP1, STRN3, and BZW (Supplemental Table S1). These candidates specifically interact with GTP-bound RhoA but not the GDP-bound form. For example, ACAT1 is important in pathways for the synthesis and degradation of ketone bodies and for the degradation of 2-methylacetoacetyl-CoA (Haapalainen *et al.*, 2007). FILIP negatively controls the function of filamin A through the degradation of filamin A, leading to the onset of neocortical migration from the ventricular zone (Sato and Nagano, 2005). Although we cannot exclude the possibility that these candidates can indirectly interact with GTP-bound RhoA, they provide us with a useful platform with which to further understand RhoA functions. It should be noted that there are several intriguing proteins, such as SLK, VAT1, PLCB4, and ACSL1, that interact with both GTP- and GDP-bound RhoA but not the GST control and could be novel types of RhoA regulators. Detailed analyses of these putative effectors and partners are underway.

MATERIALS AND METHODS

Materials and chemicals

The cDNA encoding mouse SHIP2 was kindly provided by M. Matsuda (Kyoto University, Kyoto, Japan). The pCAGGS vector was kindly provided by M. Nakafuku (Cincinnati Children's Hospital, Cincinnati, OH). The antibodies used were as follows: monoclonal anti-GFP (Roche Diagnostics, Mannheim, Germany); polyclonal anti-GFP (MBL, Nagoya, Japan); monoclonal anti-SHIP2 and anti-HA (Cell Signaling Technology, Beverly, MA); polyclonal anti-INPPL1 (Abcam, Cambridge, United Kingdom); monoclonal anti-PI(3,4,5)P₃ (Echelon Bioscience, Salt Lake City, UT); monoclonal anti-RhoA

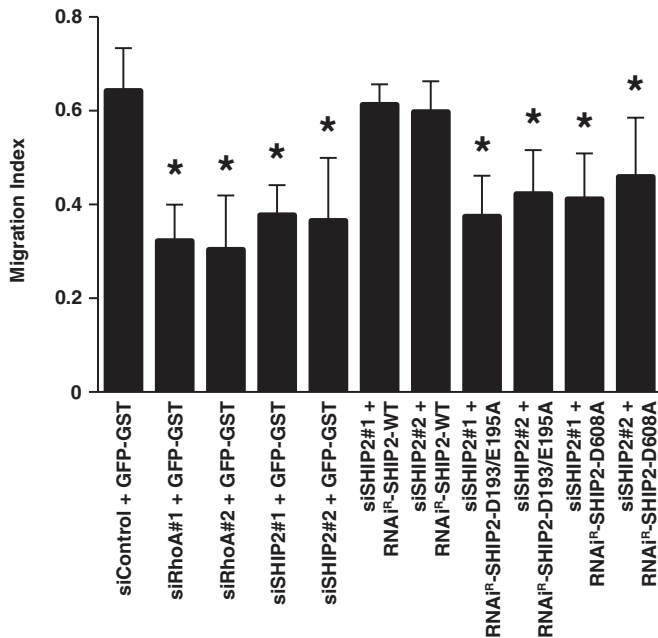


FIGURE 7: Requirement of the RhoA-binding activity of SHIP2 for cell migration. U251 cells transfected with siRNA along with the indicated plasmids were subjected to the Boyden chamber assay. The cells were allowed to migrate for 2 h. Cells were fixed and stained with the anti-GFP antibody. All results are representative of at least three independent experiments. Asterisks indicate a difference from the value of control cells at $p < 0.01$. Error bars indicate \pm SD. At least 300 EGFP-positive cells were counted per experiment.

and anti-SHIP1, polyclonal anti-SHIP2 and anti-RhoGDI (Santa Cruz Biotechnology, Santa Cruz, CA); polyclonal anti-ACAT1 (GeneTex, Irvine, CA); monoclonal anti- α -tubulin (Sigma-Aldrich, St. Louis, MO); monoclonal anti-myc (Wako Pure Chemical Industries, Osaka, Japan); and monoclonal anti-N-cadherin (BD Biosciences, San Jose, CA). The polyclonal anti-Rho-kinase antibody was prepared as previously described (Katoh *et al.*, 2001). The polyclonal anti-GST antibody was produced as previously described (Nishimura *et al.*, 2004). Fibronectin was purchased from BD Biosciences. Y-27632 was from Enzo Life Sciences (Farmingdale, NY). Wortmannin and LY294002 were from Calbiochem (San Diego, CA). The Duolink II Detection Kit with PLA PLUS and MINUS Probes for mouse and rabbit were purchased from Olink Bioscience (Uppsala, Sweden). (\pm)-3-Hydroxy-3-methyl-5-pentanolide was purchased from Wako Pure Chemical Industries. Purified phosphatidylserine was purchased from Avanti Polar Lipids, (Alabaster, AL). PI(3,4,5)P₃ was obtained from CellSignals (Columbus, OH). siRNA sequences were as follows: SHIP2#1, 5'-GGUGUUUGACCAGCAGAGC-3'; control, 5'-CAGUCGCGUUU-GCGACUGG-3'. These siRNAs with dTdT overhangs at each 3' terminus were obtained from Greiner-Japan (Tokyo, Japan). siRNAs with dTdT overhangs at each 3' terminus to SHIP2#2 and RhoA were purchased from Sigma-Aldrich: SHIP2#2, SASI_Hs01_00013990; RhoA#1, 5'-AGCAGGUAGAGUUGGCUUU-3'; RhoA#2, 5'-GGAUC-UUCGGAUGAUGAG-3'. Other materials and chemicals were obtained from commercial sources.

Plasmid constructs

The cDNA encoding full-length PTEN was cloned from a human fetal brain cDNA library (Clontech Laboratories, Palo Alto, CA). RhoA and SHIP2 fragments were amplified by PCR and subcloned

into pGEX (GE Biohealthcare Bioscience, Piscataway, NJ), pMAL (New England Biolabs, Beverly, MA), pCAGGS-myc, pEGFP (Takara, Otsu, Japan), pmCherry, pEF-BOS-GST, and pEF-BOS-HA vectors. pMitoEGFP vector was prepared as previously described (Rojo *et al.*, 2002). RhoA-A37L63, RhoA-L63, RhoA-L63S190, Rac1-L61, Cdc42-L61, SHIP2-D608A, SHIP2-D193/E195A, SHIP2-S202/N203A, SHIP2-R216/R217A, and SHIP2-D223/K224A cDNAs were generated by site-directed mutagenesis. siRNA-resistant SHIP2 mutants were generated by site-directed mutagenesis that introduced silent mutations within the siRNA target sequence. All fragments were confirmed by DNA sequencing.

Protein purification

GST- and MBP-tagged proteins were produced in BL21 (DE3) *Escherichia coli* cells and purified on glutathione-Sepharose 4B beads (GE Biohealthcare Bioscience) and amylose resin (New England Biolabs), respectively. GST-RhoA-WT for phosphatase assay was produced in Sf9 cells with a baculovirus system and purified as previously described (Mizuno *et al.*, 1991). In brief, GST-RhoA-WT-expressing Sf9 cells (1×10^8 cells) were suspended with 10 ml of homogenate buffer (10 mM Tris-HCl, pH 7.5, 1 mM dithiothreitol [DTT], 10 mM MgCl₂, 100 μ M (*p*-aminophenyl) methanesulfonyl fluoride, and 10 μ g/ml leupeptin). This suspension was sonicated and centrifuged at $100,000 \times g$ for 1 h at 4°C. The posttranslationally processed form of GST-RhoA was purified from the membrane fraction. The $100,000 \times g$ pellet was resuspended in buffer (20 mM Tris-HCl, pH 8.0, 1 mM EDTA, 1 mM DTT, 5 mM MgCl₂, and 0.6% 3-[(3-cholamidopropyl)dimethylammonio]-1-propanesulfonate [CHAPS]), stirred for 30 min, and then centrifuged at $100,000 \times g$ for 1 h at 4°C. The supernatant was purified on glutathione-Sepharose 4B beads. Recombinant Flag-tagged SHIP2 protein was purified as previously described (Hasegawa *et al.*, 2011).

Preparation of the rat heart cytosolic fraction

Rat heart (30 g) was quickly frozen with liquid nitrogen and pulverized with a Cryo-Press (15 s \times 8; Microtec Co., Chiba, Japan). The frozen heart powder was homogenized in 100 ml of homogenizing buffer (25 mM Tris-HCl, pH 7.5, 5 mM EDTA, 1 mM DTT, 5 mM MgCl₂, 500 mM NaCl, 100 μ M (*p*-aminophenyl)methanesulfonyl fluoride, 2 μ g/ml leupeptin, and 10% sucrose) and centrifuged at $20,000 \times g$ for 30 min at 4°C. The supernatant was centrifuged at $100,000 \times g$ for 1 h at 4°C. The supernatant was dialyzed three times against buffer A (20 mM Tris-HCl, pH 7.5, 1 mM EDTA, 1 mM DTT, and 5 mM MgCl₂). After dialysis, the cytosolic fraction was centrifuged at $20,000 \times g$ for 1 h at 4°C. Saturated ammonium sulfate was then added to a final concentration of 60% saturation. After centrifugation at $20,000 \times g$ for 1 h at 4°C, the precipitate was dissolved in 10 ml of buffer A, dialyzed three times against buffer A, and used as the cytosolic fraction.

Affinity column chromatography

Affinity column chromatography was performed as previously described (Hikita *et al.*, 2009). Briefly, the rat heart cytosol fraction was loaded onto a glutathione-Sepharose 4B affinity column on which 5 nmol of GST, GDP-GST-RhoA, GTP γ S-GST-RhoA, GST-RhoA-N19, or GST-RhoA-L63 was immobilized. The guanine nucleotide-bound forms of GST-RhoA were made by incubating GST-RhoA for 20 min at 30°C with 150 μ M GDP or GTP γ S in a reaction mixture (50 mM Tris-HCl, pH 7.5, 10 mM EDTA, 1 mM DTT, and 5 mM MgCl₂). After washing of the columns three times with buffer A and three times with buffer A containing 50 mM NaCl, the bound proteins were

eluted three times with buffer A containing 1 M NaCl. The first eluates were subjected to SDS-PAGE, and proteins were detected by silver staining.

Mass spectrometry

The proteins in the eluate were digested by trypsin for 16 h at 37°C after reduction, alkylation, demineralization, and concentration. Nano-electrospray tandem mass analysis was performed using an LTQ Orbitrap XL mass spectrometry system (ThermoFisher Scientific, Waltham, MA) combined with a Paradigm MS4 HPLC System (Michrom BioResources, Auburn, CA). Samples were injected onto the Paradigm MS4 HPLC System equipped with a Magic C18AQ column 0.1 mm in diameter and 50 or 150 mm in length (Michrom BioResources). Reverse-phase chromatography was performed with a linear gradient (0 min, 5% B; 100 min, 50% B) of solvent A (2% acetonitrile with 0.1% formic acid) and solvent B (90% acetonitrile with 0.1% formic acid) at an estimated flow rate of 1 μ l/min. Ionization was performed with an ADVANCE Captive Spray Source (Michrom BioResources) with a capillary voltage of 1.6 kV and temperature of 150°C. A precursor ion scan was carried out using mass-to-charge ratio (*m/z*) of 400–2000 before MS/MS analysis. Multiple MS/MS spectra were submitted to the Mascot program, version 2.3.02 (Matrix Science, Boston, MA), for the MS/MS ion search.

Protein identification

Peptides and proteins were searched against the Swiss Prot database (Swiss Prot_2010_09) by Mascot. Search parameters for Mascot included the following: variable modifications carbamidomethyl (C) and oxidation (M); mass values, monoisotopic; protein mass, unrestricted; peptide mass tolerance, 10 ppm; fragment mass tolerance, 0.8 Da; max missed cleavages, 1; instrument type, ESI-TRAP. Scaffold including X! Tandem, version 3.0 (Proteome Software, Portland, OR), was used for validation. Protein identifications were accepted if they could be established at >95.0% probability and contained at least two identified peptides.

In vitro binding assays

In vitro binding assays were performed as previously described (Nishimura *et al.*, 2004). Briefly, deletion mutants were immobilized separately onto glutathione-Sepharose 4B beads. The immobilized beads were incubated with MBP-SHIP2 deletion mutants in buffer A containing 50 mM NaCl, 0.1% NP-40, and 0.2 mg/ml bovine serum albumin (BSA) for 1 h at 4°C. Beads were washed five times with buffer A containing 50 mM NaCl and 0.1% NP-40 and then suspended in SDS-PAGE sample buffer. The bound proteins were subjected to SDS-PAGE, and proteins were detected by silver staining. For pull-down assay, the immobilized beads or glutathione-Sepharose 4B beads were incubated with COS7 cell lysate transfected with the indicated plasmid in lysis buffer (50 mM Tris-HCl, pH 7.5, 1 mM ethylene glycol tetraacetic acid [EGTA], 1 mM DTT, 10 mM MgCl₂, 150 mM NaCl, 1% NP-40, 100 μ M (*p*-amidinophenyl)methanesulfonyl fluoride, 2 μ g/ml leupeptin, and 2 μ g/ml aprotinin) for 1 h at 4°C. The beads were washed three times with lysis buffer, and then the washed beads were suspended in SDS-PAGE sample buffer. The bound proteins were subjected to an immunoblot analysis with the indicated antibodies.

Localization of SHIP2 regulated by RhoA in U251 cells

The subcellular localization of SHIP2 and RhoA was examined as previously described (Hinoi *et al.*, 1996). In brief, U251 cells transfected with the indicated plasmids were suspended in lysis buffer (50 mM Tris-HCl, pH 7.5, 1 mM EGTA, 1 mM DTT, 5 mM MgCl₂,

100 μ M (*p*-amidinophenyl)methanesulfonyl fluoride, 2 μ g/ml leupeptin, and 2 μ g/ml aprotinin), sonicated, and centrifuged at 700 \times g for 5 min. The homogenate was centrifuged at 100,000 \times g for 30 min. The supernatant was used as the cytosol fraction. The pellet was resuspended in lysis buffer containing 1% NP-40, rocked for 1 h, and then centrifuged at 100,000 \times g for 30 min. The supernatant was used as the membrane fraction. Aliquots of the cytosol and membrane fractions were subjected to SDS-PAGE and probed with the anti-myc or HA antibody.

In vitro phosphoinositide phosphatase assay

Phosphoinositide phosphatase activities were examined as previously described (Maehama and Dixon, 1998). In brief, phosphatase assay was performed at 37°C in buffer consisting of 50 mM 4-(2-hydroxyethyl)-1-piperazineethanesulfonic acid-NaOH, pH 7.4, 5 mM MgCl₂, 2 mM DTT, 50 μ M PI(3,4,5)P₃, 0.5 mM phosphatidylserine, 0.05% CHAPS, and 0.13 μ M Flag-SHIP2 in the presence or absence of 1.2 μ M GST, GDP-GST-RhoA, or GTP γ S-GST-RhoA for 5 min. The reaction was terminated by the addition of 0.1 M EDTA. Released free phosphate was detected with BIOMOL GREEN (Enzo Life Sciences).

GTP-Rho pull-down assay

The activity of RhoA was determined by pull-down assay with the GST-Rho-binding domain of Rhotekin (GST-Rhotekin-RBD) as previously described (Mori *et al.*, 2009). In brief, the cells were washed with ice-cold phosphate-buffered saline (PBS) and lysed in lysis buffer (50 mM Tris-HCl, pH 7.5, 1 mM EGTA, 10 mM MgCl₂, 500 mM NaCl, 0.5% NP-40, 0.1 mM (*p*-amidinophenyl)methanesulfonyl fluoride, 2.5 mg/ml aprotinin, and 2.5 μ g/ml leupeptin) containing 20 μ g of GST-Rhotekin-RBD. The lysates were centrifuged at 20,000 \times g for 3 min at 4°C, and the supernatants were incubated with glutathione-Sepharose 4B beads for 30 min at 4°C. The beads were washed with an excess of lysis buffer and then eluted with SDS-sample buffer. The eluates were subjected to SDS-PAGE, followed by immunoblot analysis with the anti-RhoA antibody.

Cell culture and transfection

U251 and COS7 cells were maintained in DMEM (Sigma-Aldrich) supplemented with 10% fetal bovine serum (FBS; SAFC Biosciences, St. Louis, MO). MDA-MB-231 cells were maintained in Leibovitz's L-15 Medium (Invitrogen, Carlsbad, CA) supplemented with 10% FBS. U251 cells were transfected with plasmids or siRNA by Oligofectamine or Lipofectamine LTX (Invitrogen) or by Amaxa Nucleofector (Lonza, Basel, Switzerland) according to the manufacturers' protocols. COS7 cells were transfected by Lipofectamine 2000 or Lipofectamine (Invitrogen) according to the manufacturer's protocols. MDA-MB-231 cells were transfected with siRNA by Lipofectamine RNAiMAX (Invitrogen) or plasmids by Neon Transfection System (Invitrogen) according to the manufacturer's protocols.

Immunofluorescence analysis

U251 cells were fixed with PBS containing 3.7% formaldehyde for 10 min at room temperature (RT), followed by permeabilization with 0.2% Triton X-100 for 10 min at RT. After washing with PBS, the cells were blocked with 1% BSA (Nacalai Tesque, Kyoto, Japan) for 30 min at RT and incubated with primary antibody for 1 h at RT. For anti-RhoA staining, the cells were fixed with ice-cold 10% trichloroacetic acid for 15 min at 4°C and then permeabilized with 0.1% Triton X-100 for 10 min at RT. After washing with PBS, cells were incubated with primary antibody for 1 h at RT. The secondary antibodies were Alexa 488- and 555-conjugated antibodies against

mouse immunoglobulin G (IgG) or rabbit IgG (Invitrogen). For anti-PI(3,4,5)P₃ staining in U251 cells, cells were fixed with 4% paraformaldehyde overnight at 4°C, followed by permeabilization for 45 min with PBS containing 10% normal donkey serum and 0.5% saponin, overnight incubation with the anti-PI(3,4,5)P₃ antibody at 4°C, and detection by overnight treatment using Alexa 555–conjugated antibody against mouse IgG at 4°C. For anti-PI(3,4,5)P₃ staining in MDA-MB-231 cells, we followed a previous protocol (Yip *et al.*, 2008). In brief, cells, fixed/permeabilized by 4% paraformaldehyde/0.1% glutaraldehyde in 0.15 mg/ml saponin solution for 1 h at 37°C were stained sequentially with the anti-PI(3,4,5)P₃ antibody for 1 h and the Alexa 555–conjugated secondary antibody for 45 min. Confocal images were recorded by LSM780, by LSM5 Pascal, by LSM5 built around Axio Observer Z1, Axiovert 200M, or 100M with Plan-Apochromat 20x (numerical aperture [NA] 0.75), Plan-Apochromat 20x (NA 0.8), Plan-NEO Fluor 40x (NA 0.75), C-Apochromat 40x (NA 1.2), or Plan Apochromat 63x (NA 1.40) lenses under the control of LSM software (Carl Zeiss, Jena, Germany) or by a Nikon A1 confocal laser scanning microscope built around ECLIPSE Ti with CFI Apo 40xWILS (NA 1.25), Plan Apo VC 60xWI (NA 1.2), or Plan Apo VC 60x (NA 1.4) lenses under the control of NIS-elements software (Nikon, Tokyo, Japan). Images were processed using Photoshop (Adobe, San Jose, CA). Duolink images were processed using NIS-elements software and Photoshop.

Proximity ligation in situ assay (Duolink)

The interactions between SHIP2 and RhoA in U251 cells were analyzed using the Duolink II proximity ligation in situ assay (Fredriksson *et al.*, 2002; Soderberg *et al.*, 2006) according to the manufacturer's instructions. The anti-INPPL1 rabbit polyclonal antibody was combined with the anti-RhoA mouse monoclonal antibody. Fluorescence spots generated were automatically counted, and the average number of spots per cell was calculated using MetaMorph (Molecular Devices, Downingtown, PA).

Quantification of polarity

Polarity was defined as cells with a single leading edge as evaluated by phalloidin staining. Quantification of polarity was performed with at least three independent experiments. The evaluations were performed with at least 100 cells in each experiment.

Boyden chamber assay

The Boyden chamber assay was performed as previously described (Watanabe *et al.*, 2009). Briefly, siRNA was transfected into U251 cells with the indicated plasmid. Cell migration assays were performed using Transwell plates (pore size, 8 µm; HTS FluoroBlok Insert; BD Biosciences). The undersurface of the membrane was coated for 1 h at RT with 10 µg/ml fibronectin diluted in distilled water. The cells were seeded in the upper chamber (1 × 10⁴ per well) in 500 µl of DMEM with 0.1% BSA. DMEM supplemented with 0.1% BSA and 10 ng/ml EGF was added to the lower chamber. The cells were allowed to migrate for 2 h. After fixation, both nonmigrated and migrated EGFP-positive cells were counted by EGFP fluorescence, and the ratio of migrated cells to total (migrated plus nonmigrated) cells was calculated and determined as the migration index. At least 300 EGFP-positive cells were counted in each group for each experiment. The results were normalized and expressed as a migration index.

Statistical analysis

Student's *t* test and one-way analysis of variance (ANOVA) were performed after data were confirmed to satisfy the criteria of normal

distribution and equal variance. If the overall ANOVA was significant, we performed a post hoc test. Dunnett's multiple comparison test was carried out.

ACKNOWLEDGMENTS

We thank M. Matsuda (Kyoto University, Kyoto, Japan) for kindly providing SHIP2 cDNA and helpful discussion. We thank M. Inagaki (Aichi Cancer Center Research Institute, Nagoya, Japan) for kindly providing U251 cells. We thank Frank B. Gertler (Massachusetts Institute of Technology, Cambridge, MA) and T. Nishimura (RIKEN Center for Developmental Biology, Kobe, Japan) for helpful discussions. We thank F. Ishidate for help with acquiring and analyzing images and A. Iwamatsu (Protein Research Network, Kanagawa, Japan), Y. Yamakawa (Division for Medical Research Engineering, Nagoya University, Japan), ThermoFisher Scientific, and AMR (Tokyo, Japan) for mass spectrometric analysis. We also thank all members of the Kaibuchi lab for discussions and technical support, Y. Kanazawa for technical assistance, and T. Ishii for secretarial assistance. We also thank T. Watanabe for helpful discussions, T. Namba, S. Nakamura, K. Kuroda, and Y. Funahashi (our laboratory) for help with microscopy, and H. Shohag and X. Zhang for technical support. We acknowledge the Division of Medical Research Engineering of the Nagoya University Graduate School of Medicine for the use of ImageQuant LAS 4010 (GE Biohealthcare Bioscience) and Nikon-A1 microscopy, and we thank the Radioisotope Center Medical Branch, Nagoya University School of Medicine (Technical Staff, N. Hamada and Y. Nakamura). This research was supported in part by Nagoya University Global COE Program, Integrated Functional Molecular Medicine for Neuronal and Neoplastic Disorders, Grants-in-Aid for Scientific Research (S; 20227006) and (C; 23590357) from the Ministry of Education, Culture, Sports, Science and Technology of Japan, and the Kyosaidan Foundation, the Nagono Medical Foundation, and the Japan Foundation for Applied Enzymology.

REFERENCES

- Amano M, Nakayama M, Kaibuchi K (2010). Rho-kinase/ROCK: a key regulator of the cytoskeleton and cell polarity. *Cytoskeleton* (Hoboken) 67, 545–554.
- Blero D, Zhang J, Pesesse X, Payrastra B, Dumont JE, Schurmans S, Erneux C (2005). Phosphatidylinositol 3,4,5-trisphosphate modulation in SHIP2-deficient mouse embryonic fibroblasts. *FEBS J* 272, 2512–2522.
- Blumenstein L, Ahmadian MR (2004). Models of the cooperative mechanism for Rho effector recognition: implications for RhoA-mediated effector activation. *J Biol Chem* 279, 53419–53426.
- Cantley LC (2002). The phosphoinositide 3-kinase pathway. *Science* 296, 1655–1657.
- Di Paolo G, De Camilli P (2006). Phosphoinositides in cell regulation and membrane dynamics. *Nature* 443, 651–657.
- Etienne-Manneville S (2008). Polarity proteins in migration and invasion. *Oncogene* 27, 6970–6980.
- Fredriksson S, Gullberg M, Jarvius J, Olsson C, Pietras K, Gustafsdottir SM, Ostman A, Landegren U (2002). Protein detection using proximity-dependent DNA ligation assays. *Nat Biotechnol* 20, 473–477.
- Haapalainen AM, Merilainen G, Pirila PL, Kondo N, Fukao T, Wierenga RK (2007). Crystallographic and kinetic studies of human mitochondrial acetoacetyl-CoA thiolase: the importance of potassium and chloride ions for its structure and function. *Biochemistry* 46, 4305–4321.
- Han J, Luby-Phelps K, Das B, Shu X, Xia Y, Mosteller RD, Krishna UM, Falck JR, White MA, Broek D (1998). Role of substrates and products of PI 3-kinase in regulating activation of Rac-related guanosine triphosphatases by Vav. *Science* 279, 558–560.
- Hasegawa J, Tokuda E, Tenno T, Tsujita K, Sawai H, Hiroaki H, Takenawa T, Itoh T (2011). SH3YL1 regulates dorsal ruffle formation by a novel phosphoinositide-binding domain. *J Cell Biol* 193, 901–916.

- Hikita T *et al.* (2009). Proteomic analysis reveals novel binding partners of dysbindin, a schizophrenia-related protein. *J Neurochem* 110, 1567–1574.
- Hinoi T, Kishida S, Koyama S, Ikeda M, Matsuura Y, Kikuchi A (1996). Post-translational modifications of Ras and Ral are important for the action of Ral GDP dissociation stimulator. *J Biol Chem* 271, 19710–19716.
- Horiguchi K, Hanada T, Fukui Y, Chishti AH (2006). Transport of PIP₃ by GAKIN, a kinesin-3 family protein, regulates neuronal cell polarity. *J Cell Biol* 174, 425–436.
- Iden S, Collard JG (2008). Crosstalk between small GTPases and polarity proteins in cell polarization. *Nat Rev Mol Cell Biol* 9, 846–859.
- Itoh RE, Kurokawa K, Ohba Y, Yoshizaki H, Mochizuki N, Matsuda M (2002). Activation of rac and cdc42 video imaged by fluorescent resonance energy transfer-based single-molecule probes in the membrane of living cells. *Mol Cell Biol* 22, 6582–6591.
- Jaffe AB, Hall A (2005). Rho GTPases: biochemistry and biology. *Annu Rev Cell Dev Biol* 21, 247–269.
- Katoh K, Kano Y, Amano M, Onishi H, Kaibuchi K, Fujiwara K (2001). Rho-kinase-mediated contraction of isolated stress fibers. *J Cell Biol* 153, 569–584.
- Kimura K *et al.* (1996). Regulation of myosin phosphatase by Rho and Rho-associated kinase (Rho-kinase). *Science* 273, 245–248.
- Kraynov VS, Chamberlain C, Bokoch GM, Schwartz MA, Slabaugh S, Hahn KM (2000). Localized Rac activation dynamics visualized in living cells. *Science* 290, 333–337.
- Kunisaki Y *et al.* (2006). DOCK2 is a Rac activator that regulates motility and polarity during neutrophil chemotaxis. *J Cell Biol* 174, 647–652.
- Kurokawa K, Matsuda M (2005). Localized RhoA activation as a requirement for the induction of membrane ruffling. *Mol Biol Cell* 16, 4294–4303.
- Lee CS, Choi CK, Shin EY, Schwartz MA, Kim EG (2010). Myosin II directly binds and inhibits Dbl family guanine nucleotide exchange factors: a possible link to Rho family GTPases. *J Cell Biol* 190, 663–674.
- Lindsay Y, McCoull D, Davidson L, Leslie NR, Fairservice A, Gray A, Lucocq J, Downes CP (2006). Localization of agonist-sensitive PtdIns(3,4,5)P₃ reveals a nuclear pool that is insensitive to PTEN expression. *J Cell Sci* 119, 5160–5168.
- Maehama T, Dixon JE (1998). The tumor suppressor, PTEN/MMAC1, dephosphorylates the lipid second messenger, phosphatidylinositol 3,4,5-trisphosphate. *J Biol Chem* 273, 13375–13378.
- Maesaki R, Ihara K, Shimizu T, Kuroda S, Kaibuchi K, Hakoshima T (1999). The structural basis of Rho effector recognition revealed by the crystal structure of human RhoA complexed with the effector domain of PKN/PRK1. *Mol Cell* 4, 793–803.
- Mandl A, Sarkes D, Carricaburu V, Jung V, Rameh L (2007). Serum withdrawal-induced accumulation of phosphoinositide 3-kinase lipids in differentiating 3T3-L6 myoblasts: distinct roles for Ship2 and PTEN. *Mol Cell Biol* 27, 8098–8112.
- Mizuno T, Kaibuchi K, Yamamoto T, Kawamura M, Sakoda T, Fujioka H, Matsuura Y, Takai Y (1991). A stimulatory GDP/GTP exchange protein for smg p21 is active on the post-translationally processed form of c-Ki-ras p21 and rhoA p21. *Proc Natl Acad Sci USA* 88, 6442–6446.
- Mori K, Amano M, Takefuji M, Kato K, Morita Y, Nishioka T, Matsuura Y, Murohara T, Kaibuchi K (2009). Rho-kinase contributes to sustained RhoA activation through phosphorylation of p190A RhoGAP. *J Biol Chem* 284, 5067–5076.
- Nakatsu F, Perera RM, Lucast L, Zoncu R, Domin J, Gertler FB, Toomre D, De Camilli P (2010). The inositol 5-phosphatase SHIP2 regulates endocytic clathrin-coated pit dynamics. *J Cell Biol* 190, 307–315.
- Nakayama M, Goto TM, Sugimoto M, Nishimura T, Shinagawa T, Ohno S, Amano M, Kaibuchi K (2008). Rho-kinase phosphorylates PAR-3 and disrupts PAR complex formation. *Dev Cell* 14, 205–215.
- Narumiya S, Tanji M, Ishizaki T (2009). Rho signaling, ROCK and mDia1, in transformation, metastasis and invasion. *Cancer Metastasis Rev* 28, 65–76.
- Nishimura T, Kato K, Yamaguchi T, Fukata Y, Ohno S, Kaibuchi K (2004). Role of the PAR-3-KIF3 complex in the establishment of neuronal polarity. *Nat Cell Biol* 6, 328–334.
- Nishio M *et al.* (2007). Control of cell polarity and motility by the PtdIns(3,4,5)P₃ phosphatase SHIP1. *Nat Cell Biol* 9, 36–44.
- Ohta Y, Hartwig JH, Stossel TP (2006). FilGAP, a Rho- and ROCK-regulated GAP for Rac binds filamin A to control actin remodelling. *Nat Cell Biol* 8, 803–814.
- Ooms LM, Horan KA, Rahman P, Seaton G, Gurung R, Kethesparan DS, Mitchell CA (2009). The role of the inositol polyphosphate 5-phosphatases in cellular function and human disease. *Biochem J* 419, 29–49.
- Owen D, Lowe PN, Nietlispach D, Brosnan CE, Chirgadze DY, Parker PJ, Blundell TL, Mott HR (2003). Molecular dissection of the interaction between the small G proteins Rac1 and RhoA and protein kinase C-related kinase 1 (PRK1). *J Biol Chem* 278, 50578–50587.
- Peck JW, Oberst M, Bouker KB, Bowden E, Burbelo PD (2002). The RhoA-binding protein, raphilin-2, regulates actin cytoskeleton organization. *J Biol Chem* 277, 43924–43932.
- Pertz O, Hodgson L, Klemke RL, Hahn KM (2006). Spatiotemporal dynamics of RhoA activity in migrating cells. *Nature* 440, 1069–1072.
- Petrie RJ, Doyle AD, Yamada KM (2009). Random versus directionally persistent cell migration. *Nat Rev Mol Cell Biol* 10, 538–549.
- Rameh LE *et al.* (1997). A comparative analysis of the phosphoinositide binding specificity of pleckstrin homology domains. *J Biol Chem* 272, 22059–22066.
- Ridley AJ, Schwartz MA, Burridge K, Firtel RA, Ginsberg MH, Borisy G, Parsons JT, Horwitz AR (2003). Cell migration: integrating signals from front to back. *Science* 302, 1704–1709.
- Riento K, Ridley AJ (2003). Rocks: multifunctional kinases in cell behaviour. *Nat Rev Mol Cell Biol* 4, 446–456.
- Rojo M, Legros F, Chateau D, Lombes A (2002). Membrane topology and mitochondrial targeting of mitofusins, ubiquitous mammalian homologs of the transmembrane GTPase Fzo. *J Cell Sci* 115, 1663–1674.
- Sato M, Nagano T (2005). Involvement of filamin A and filamin A-interacting protein (FILIP) in controlling the start and cell shape of radially migrating cortical neurons. *Anat Sci Int* 80, 19–29.
- Sato M, Ueda Y, Takagi T, Umezawa Y (2003). Production of PtdInsP₃ at endomembranes is triggered by receptor endocytosis. *Nat Cell Biol* 5, 1016–1022.
- Shimizu T, Ihara K, Maesaki R, Amano M, Kaibuchi K, Hakoshima T (2003). Parallel coiled-coil association of the RhoA-binding domain in Rho-kinase. *J Biol Chem* 278, 46046–46051.
- Soderberg O *et al.* (2006). Direct observation of individual endogenous protein complexes in situ by proximity ligation. *Nat Methods* 3, 995–1000.
- Vega FM, Fruhwirth G, Ng T, Ridley AJ (2011). RhoA and RhoC have distinct roles in migration and invasion by acting through different targets. *J Cell Biol* 193, 655–665.
- Watanabe T *et al.* (2009). Phosphorylation of CLASP2 by GSK-3beta regulates its interaction with IQGAP1, EB1 and microtubules. *J Cell Sci* 122, 2969–2979.
- Weiger MC, Wang CC, Krajcovic M, Melvin AT, Rhoden JJ, Haugh JM (2009). Spontaneous phosphoinositide 3-kinase signaling dynamics drive spreading and random migration of fibroblasts. *J Cell Sci* 122, 313–323.
- Weng L, Enomoto A, Ishida-Takagishi M, Asai N, Takahashi M (2010). Girding for migratory cues: roles of the Akt substrate Girdin in cancer progression and angiogenesis. *Cancer Sci* 101, 836–842.
- Worthylake RA, Burridge K (2003). RhoA and ROCK promote migration by limiting membrane protrusions. *J Biol Chem* 278, 13578–13584.
- Yip SC, Eddy RJ, Branch AM, Pang H, Wu H, Yan Y, Drees BE, Neilsen PO, Condeelis JS, Backer JM (2008). Quantification of PtdIns(3,4,5)P₃ dynamics in EGF-stimulated carcinoma cells: a comparison of PH-domain-mediated methods with immunological methods. *Biochem J* 411, 441–448.